Nucl. Phys. B 1016 (2025) 116915

Contents lists available at ScienceDirect

Nuclear Physics, Section B

journal homepage: www.elsevier.com/locate/nuclphysb

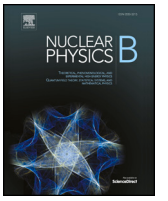

High Energy Physics – Theory

Thermodynamic behavior and phase transitions of black holes with a cloud of strings and perfect fluid dark matter

Dharm Veer Singh [a,c,1], Sudhaker Upadhyay [b,c,d,*,2], Yerlan Myrzakulov [d,*], Kairat Myrzakulov [d], Bhupendra Singh [e], Manish Kumar [e]

[a] Department of Physics, Institute of Applied Science and Humanities, GLA University, Mathura 281406, India
[b] Department of Physics, K.L.S. College, Nawada, Magadh University, Bodh Gaya, Bihar 805110, India
[c] School of Physics, Damghan University, P.O. Box 3671641167, Damghan, Iran
[d] Department of General & Theoretical Physics, L. N. Gumilyov Eurasian National University, Astana, 010008, Kazakhstan
[e] Department of Physics, Atma Ram Sanatan Dharma College, University of Delhi, Delhi 110021, India

ARTICLE INFO

Editor: Y. Lozano

ABSTRACT

This paper presents an exact black hole solution within a cloud of strings (CoS) and a perfect fluid dark matter (PFDM) field. The derived black hole solution interpolates between the AdS-charged Letelier black hole in the absence of the PFDM field and the AdS Reissner-Nordström black hole in the limiting case of the PFDM and CoS parameters. The thermodynamic properties of the black hole, including temperature, entropy, heat, and free energy, are modified in the presence of the PFDM field and CoS parameter. Furthermore, we investigate the black hole's critical points and phase structure in an extended phase space. We find that the critical temperature and pressure decrease with the CoS parameter but increase with the PFDM field. The Gibbs free energy versus temperature plot reveals a swallow-tail behavior, indicating a first-order phase transition, which terminates at a second-order phase transition.

1. Introduction

Black holes (BHs) are an excellent tool to unravel the nature of gravity and provide a rich area to explore the effect of gravity. The connection between the BHs and ordinary thermodynamics [1] has given a strong foundation for this possibility. Classically, the surface area of the BHs is identified as the entropy and leads to the identification of the law of BH thermodynamics [2]. The surface gravity is recognized as the temperature after invoking the quantum effects [3]. The BH thermodynamics is more interesting after discovering Hawking-Page phase transition (PT) [4]. This PT occurs between the hot radiation and Schwarzschild BH, giving the alternate interpretation of confinement/de-confinement in conformal field theory [5,6]. Chamblin [7,8] shows the phase transition between the small-large BH for AdS Reissner-Nordström BH, which is analogous to the liquid-gas PT.

* Corresponding authors.
E-mail addresses: veerdsingh@gmail.com (D.V. Singh), sudhakerupadhyay@gmail.com (S. Upadhyay), ymyrzakulov@gmail.com (Y. Myrzakulov), krmyrzakulov@gmail.com (K. Myrzakulov), rajbhupendra81@gmail.com (B. Singh), mkumar2@arsd.du.ac.in (M. Kumar).
[1] Visiting Associate, IUCAA, Pune, Maharashtra 411007, India.
[2] Visiting Associate, IUCAA, Pune, Maharashtra 411007, India.

https://doi.org/10.1016/j.nuclphysb.2025.116915
Received 18 January 2025; Received in revised form 15 March 2025; Accepted 17 April 2025

Available online 23 April 2025

The cosmological constant is treated as thermodynamics pressure ($\Lambda = -8\pi P$) in an extended phase space, and the corresponding conjugate quantity is thermodynamic volume [9–11]. It gives new insight into the thermodynamics of the BH. The modified first law of thermodynamics is

$$dM = TdS + \Phi dQ + PdV, \tag{1}$$

where Q is the charge, and Φ is its conjugate quantity potential. In the extended phase space phenomenon, the BH mass is interpreted as enthalpy rather than the internal energy, and the extended thermodynamics ensure that the small BH to large BH PT has the exact map to the liquid-gas PT, where the first order PT is ending at the second order one. Here we note that the Brown-York quasilocal energy, ADM mass, and Komar mass provide distinct characterizations of gravitational mass. The ADM mass, defined at spatial infinity for asymptotically flat spacetimes, represents the total energy, including gravitational radiation, and coincides with the mass parameter M in stationary vacuum solutions such as Schwarzschild and Kerr. The Komar mass, applicable in stationary spacetimes, is computed via an integral involving the time-like Killing vector and, in vacuum, satisfies $M_{\text{Komar}} = 2M_{\text{ADM}}$, reflecting gravitational binding energy. The Brown-York quasilocal energy is defined on a finite boundary and depends on the reference spacetime, making it useful for analyzing energy in finite regions, such as near the black hole horizon. While the ADM mass asymptotically approaches M, the Brown-York energy varies with the boundary choice, and the Komar mass equals M only in stationary cases.

The Van der Waals PT applies to the study of small-to-large BH phase transitions and can be extended to more complex scenarios, such as reentrant phase transitions, superfluidity, and solid-liquid phase transitions. This PT framework plays a crucial role in examining the thermodynamic properties of BHs, particularly at critical points. Understanding phase transitions in BHs provides valuable insights into the nature of these critical points and reveals additional characteristics of BH systems.

The consideration of Van der Waals-like phase transitions has been explored in various types of BHs. For instance, the phase transition in AdS Reissner-Nordström BHs was analyzed in the seminal work by Kubiznak and Mann [12]. Similarly, investigations have been conducted on regular BHs [13–21], where the PT framework is used to study the thermodynamic behavior of such solutions.

Rotating BHs have also been examined within this framework [22–25], as well as Einstein-Gauss-Bonnet (EGB) BHs [26,27], where the higher curvature corrections offer new insights into phase transitions. Studies on massive BHs [28,29], Lovelock BHs [30–34], and scalar BHs [35–37] further broaden the applicability of phase transition analysis to various gravitational theories.

Additionally, EGB regular BHs have been extensively studied for their phase structure and critical behavior [38–41], showcasing the richness of PT phenomena in a range of BH solutions. These studies underline the importance of phase transition analysis in gaining a deeper understanding of BH thermodynamics across different models and gravitational frameworks.

Motivated by this work, we are interested in studying the thermodynamic feature, including the phase structure of an exact AdS BH solution coupled with the CoS parameter surrounded by the PFDM field. We find an exact BH solution in the presence of the CoS parameter, surrounded by the PFDM field. This BH solution interpolates between the Reissner-Nordström BH when the CoS and scale parameters are absent and the Schwarzschild BH when the charge, CoS parameter, and scale parameter are all set to zero. The obtained BH solution becomes the Letelier solution [42–44] in the limit of electromagnetic charge and PFDM. The size of the BH depends on both the CoS parameter and the PFDM field, increasing with the CoS parameter and decreasing with the PFDM field. We also examine the full thermodynamics of the system, including mass, temperature, heat capacity, and free energy. The heat capacity diverges at the extremal points of temperature and Gibbs free energy.

Furthermore, we study the critical points and phase structure by analyzing the equation of state (EoS) and Gibbs free energy. The effects of the CoS source and the PFDM field on the critical points are opposite. Additionally, we identify three types of BHs within specific pressure ranges: small stable BHs for $P < P_c$, large stable BHs for $P > P_c$, and intermediate unstable BHs at $P = P_c$. The appearance of a shallow tail shape in the $G_+ - T_+$ diagram indicates a first-order phase transition occurring at the transition temperature, which decreases as the scale parameter increases.

The paper is structured as follows: In Sec. 2, we derive the BH solution in the presence of the CoS parameter and the PFDM field and analyze the corresponding horizon structure. Sec. 3 focuses on the extended thermodynamics and stability analysis of the BH. We investigate the critical points and phase structure in Sec. 4. Finally, we summarize and discuss our findings in Sec. 5.

2. Action, field equations, and BH solutions

The action of Einstein's gravity coupled with the CoS parameter surrounded by the PFDM field in the presence of AdS space-time is given by

$$S = \int d^4x\sqrt{-g}\Big[\mathcal{R} - 2\Lambda + 2\nabla_\mu\Phi\nabla^\mu\Phi - 4V(\Phi) - 4\mathcal{L}_{DM} + \mathcal{L}_{CS} - F_{\mu\nu}F^{\mu\nu}\Big] + S_{\text{CS}}, \tag{2}$$

where $\mathcal{R}$ is a curvature scalar, Λ is a cosmological constant, Φ is a phantom field, $V(\Phi)$ is a phantom field potential, $\mathcal{L}_{DM}$ is the Lagrangian density of the dark matter field, S_{CS} is the action of CoS source and $F_{\mu\nu} = \partial A_\mu - \partial A_\nu$ is the electromagnetic field tensor. The CoS source [43] is governed by the following action:

$$S_{\text{CS}} = \int_\Sigma m(-h)^{-1/2}d\gamma^0 d\gamma^1 = \int_\Sigma m\left(-\frac{1}{2}\Sigma^{\mu\nu}\Sigma_{\mu\nu}\right)^{1/2} d\lambda^0 d\lambda^1, \tag{3}$$

where m is the mass of the string, h is the determinant of the reduced metric, γ^0 is time-like coordinate and γ^1 is space-like coordinate [43]. The $\Sigma^{\mu\nu}$ is given by

$$\Sigma^{\mu\nu} = \epsilon^{ab} \frac{\partial y^\mu}{\partial \gamma^a} \frac{\partial y^\nu}{\partial \gamma^b}, \tag{4}$$

where ϵ^{ab} is the Levi-Civta tensor with the non-vanishing components $\epsilon^{01} = -\epsilon^{10} = 1$.

Variation of action (2) with respect to metric tensor ($g_{\mu\nu}$) and electromagnetic potential (A_μ) leads to the following equation of motion:

$$G_{\mu\nu} + \Lambda g_{\mu\nu} = T^{CS}_{\mu\nu} + T_{\mu\nu}, \tag{5}$$

$$\nabla_\mu (F^{\mu\nu}) = 0 \quad \text{and} \quad \nabla_\mu (* F^{\mu\nu}) = 0, \tag{6}$$

where $A_t = -Q/r$ is the non-vanishing component of electromagnetic potential. The energy-momentum tensor (EMT) for the CoS source is given by [45]

$$T^{\mu\nu}_{CS} = \frac{\rho \Sigma^{\mu\rho} \Sigma_\rho^{\ \nu}}{\sqrt{-h}} = \frac{a}{r^2} \text{diag}[1, 1, 0, 0], \tag{7}$$

where a is a CoS parameter.

Now, we write the EMT corresponding to the PFDM together with electromagnetic fields as

$$T_{\mu\nu} = 2\left[F_{\mu\gamma} F^\gamma_\nu - \frac{1}{2} g_{\mu\nu} F\right] + 2\nabla_\mu \Phi \nabla_\nu \Phi - g_{\mu\nu} \nabla_\gamma \Phi \nabla^\gamma \Phi + T^{DM}_{\mu\nu}, \tag{8}$$

where $T^{DM}_{\mu\nu}$ refers to the EMT of the PFDM field.

Now, we consider the general static and the spherically symmetric metric for finding the BH solution as

$$ds^2 = -e^{A(r)} dt^2 + e^{B(r)} dr^2 + r^2 \left(d\theta^2 + \sin^2\theta d\phi^2\right). \tag{9}$$

For the static situation, the Einstein equations read

$$G^t_t = e^{-B(r)} \left(\frac{1}{r^2} - \frac{B(r)'}{r}\right) - \frac{1}{r^2} - \Lambda r^2 = T^t_t \tag{10}$$

$$G^r_r = e^{-B(r)} \left(\frac{1}{r^2} + \frac{A(r)'}{r}\right) - \frac{1}{r^2} - \Lambda r^2 = T^r_r, \tag{11}$$

$$G^\theta_\theta = \frac{e^{-B(r)}}{2} \left(A(r)'' + \frac{A'(r)^2}{2} + \frac{A(r)' - B'(r)}{r} - \frac{A(r)' B(r)'}{2}\right) - \Lambda r^2 = T^\theta_\theta, \tag{12}$$

where prime denotes the differentiation concerning r. Here, we note that the G^θ_θ and G^ϕ_ϕ components of the Einstein field equation Eq. (5) are the same.

The components of EMT (8) are

$$T^t_t = \frac{Q^2}{r^4} + \frac{a}{r^2} + \frac{1}{2} e^{-B(r)} \Phi'^2 - V(\Phi) - \rho_{\text{DM}}, \tag{13}$$

$$T^r_r = \frac{Q^2}{r^4} + \frac{a}{r^2} - \frac{1}{2} e^{-B(r)} \Phi'^2 - V(\Phi), \tag{14}$$

$$T^\theta_\theta = \frac{1}{2} e^{-B(r)} \Phi'^2 - V(\Phi). \tag{15}$$

The EMT for the spherical coordinate for cold dark matter diag$[-\rho_{\text{DM}}, 0, 0, 0]$.

To find the BH solution that follows the condition $A(r) = -B(r)$ ($g_{tt} = -1/g_{rr}$) and $\rho_{\text{DM}} = e^{A(r)} \Phi'^2 > 0$, we set $B(r) = \ln(1 - \mathcal{U}(r))$ and substitute it into Eqs. (10) and (12). We then obtain

$$r^2 \mathcal{U}(r)'' + 2\epsilon r \mathcal{U}'(r) + 2(1 - \epsilon)\mathcal{U}(r) - \Lambda r^2 = \frac{a}{r^2} + \frac{Q^2}{r^4}, \tag{16}$$

where we have set $T^{\theta\theta} + T^{\theta\theta}_{CS} = T^{\phi\phi} + T^{\phi\phi}_{CS} = (1 - \epsilon) T^{tt} + T^{tt}_{CS}$, with a constant ϵ. The Eq. (16) exhibits the following solutions

$$\mathcal{U}(r) = \frac{2M}{r} - \frac{r^{2(1-\epsilon)}}{r} - \frac{Q^2}{r^2} + a, \qquad \epsilon \neq \frac{3}{2} \tag{17}$$

$$\mathcal{U}(r) = \frac{2M}{r} + \frac{\lambda}{r} \ln\left(\frac{r}{\lambda}\right) - \frac{Q^2}{r^2} + a, \qquad \epsilon = \frac{3}{2}, \tag{18}$$

where λ is the integration constant. The BH solution for $\epsilon = 3/2$ is given as

$$\begin{aligned} ds^2 = &-\left(1 - \frac{2M}{r} + \frac{Q^2}{r^2} - a + \frac{\lambda}{r} \ln\left[\frac{r}{\lambda}\right] + \frac{r^2}{l^2}\right) dt^2 \\ &+ \left(1 - \frac{2M}{r} + \frac{Q^2}{r^2} - a + \frac{\lambda}{r} \ln\left[\frac{r}{\lambda}\right] + \frac{r^2}{l^2}\right)^{-1} dr^2 + r^2 d\Omega^2. \end{aligned} \tag{19}$$

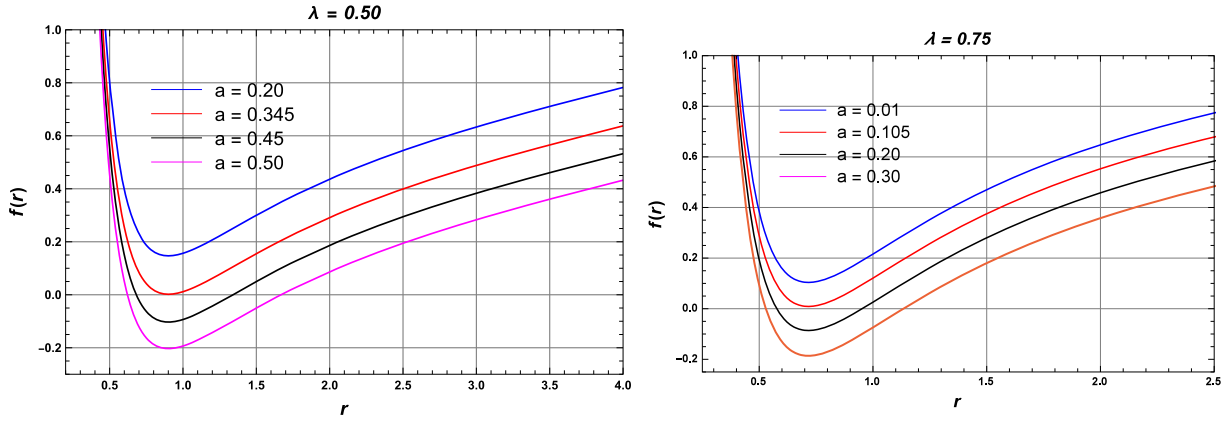

Fig. 1. The plot of the metric function $f(r)$ versus r for various values of the CoS parameter. In the left panel, the curves correspond to $a = 0.20$ (Blue line), $a = 0.345$ (Red line), $a = 0.45$ (Black line), and $a = 0.50$ (Pink line) for a fixed scale parameter $\lambda = 0.5$. In the right panel, the curves represent $a = 0.01$ (Blue line), $a = 0.105$ (Red line), $a = 0.20$ (Black line), and $a = 0.30$ (Pink line) with a fixed scale parameter $\lambda = 0.75$. The parameters are fixed in both cases as $M = Q = 1$ and $l = 10$.

Table 1
The numerical values of Cauchy horizon (r_-), event horizon (r_+) and $\delta = r_+ - r_-$ for various values of CoS parameter for $\lambda = 0.5$ and $\lambda = 0.75$ with fixed value of mass ($M = Q = 1$) and AdS length scale $l = 10$.

$\lambda = 0.50$				$\lambda = 0.75$			
a	r_-	r_+	δ	a	r_-	r_+	δ
0.345	0.922	0.922	0.0	0.105	0.718	0.718	0.0
0.4	0.734	1.194	0.406	0.408	0.504	1.321	0.323
0.45	0.674	1.32	0.646	0.45	0.487	1.427	0.940
0.5	0.642	1.503	0.861	0.50	0.467	1.538	1.071

The BH solution (19) with an electromagnetic field, CoS parameter, and PFDM field (19) arose as the solution of the Einstein field equations (10) to (12). This BH solution (19) characterized by the five parameters mass (M), charge (Q), CoS parameter (a), scale parameter (λ) and cosmological constant (Λ related to AdS length l by $\Lambda = -3/l^2$). The obtained BH solution (19) interpolates with the charged Letelier BH in the absence of scale parameter (λ). In the limit of charge ($Q = 0$), the BH solution (19) reduces to

$$ds^2 = -\left(1 - \frac{2M}{r} + -a + \frac{\lambda}{r}\ln\left[\frac{r}{\lambda}\right] + \frac{r^2}{l^2}\right)dt^2 + \left(1 - \frac{2M}{r} - a + \frac{\lambda}{r}\ln\left[\frac{r}{\lambda}\right] + \frac{r^2}{l^2}\right)^{-1} dr^2 + r^2 d\Omega^2. \tag{20}$$

The BH solution (19) reduces to the Reissner-Nordeström BH for $\lambda = a = 0$, Letelier BH in the limit of ($\lambda = 0, Q = 0$) and Schwarzschild BH for $\lambda = Q = a = 0$. This solution (19) is asymptotically AdS due to the negative cosmological constant. The solution (19) signals that the event horizons can be obtained by solving $f(r) = 0$ and finding its largest positive root. However, Eq. (19) can not be solved analytically. So, we plot fig. (19) for the different values of CoS parameter a with a fixed value of scale parameter (λ) as depicted in the Fig. 1 and the numerical values of the horizons are depicted in the Table 1.

From the plot 1, the BH has two horizons viz. Cauchy (r_-) a d event horizon (r_-) depends upon the parameters (M, Q, a, λ) and AdS length (l). The numerical values of the horizons with different values of a for fixed values of $\lambda = 0.50$ and $\lambda = 0.75$ are presented in Table 1. The critical value of CoS parameter (for $\lambda = 0.50$) is 0.345. The obtained BH solution has two horizon ($\lambda > \lambda_c$) and no horizon for ($\lambda < \lambda_c$).

In Fig. 1 and Table 1, we notice that the size of the BH increases with the increase of the value of the CoS parameter and decreases with the increase in the scale parameter (λ). In other words, e can say that the effects of the scale parameter (λ) and CoS parameter (a) on the size of the BH are in contrast.

3. Mass, temperature and (local and global) stability

In this section, we study the thermodynamics of BH in terms of horizon radius (r_+). The mass of the BH can be calculated simply by using the $f(r) = 0$ as

$$M_+ = \frac{r_+}{2}\left(1 + \frac{Q^2}{r_+^2} - a + \frac{r_+^2}{l^2} + \frac{\lambda}{2r_+}\log\left[\frac{r_+}{\lambda}\right]\right). \tag{21}$$

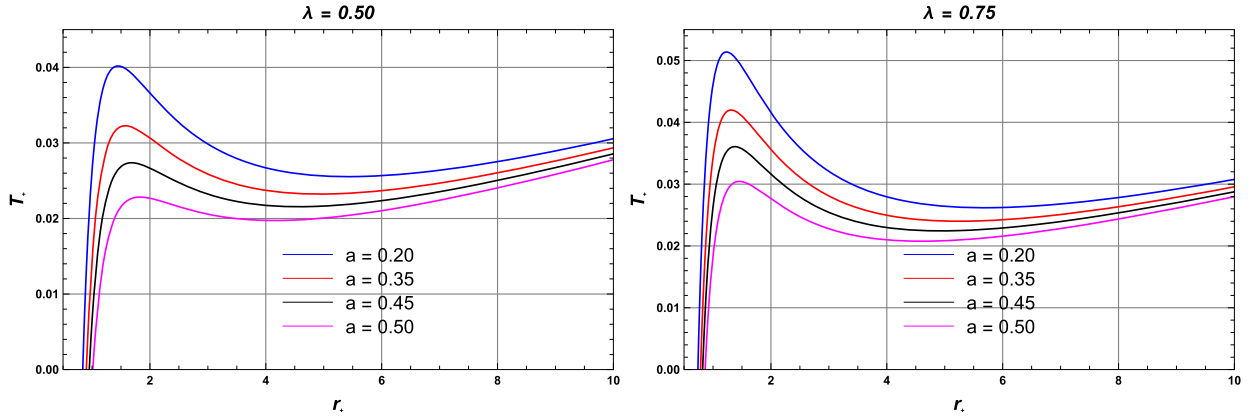

Fig. 2. The plot of T_+ versus the horizon radius r_+ for various values of the CoS parameter. In the left panel, we consider $a = 0.20$ (Blue line), $a = 0.35$ (Red line), $a = 0.45$ (Black line), and $a = 0.50$ (Pink line) with a fixed scale parameter $\lambda = 0.5$. In the right panel, we consider the same values of a with a fixed scale parameter $\lambda = 0.75$. Both cases are plotted for fixed values of $M = Q = 1$ and $l = 10$.

Here, it is evident that four parameters, namely, charge (Q), CoS parameter (a), scale parameter (λ), and cosmological constant (Λ), characterize the mass of the BH solution. The BH mass (21) reduces to AdS charged Letelier BH mass in the limit of $\lambda \to 0$, AdS Letelier BH mass in the absence of both $Q = 0$ and $\lambda \to 0$, AdS Reissner-Nordström BH in the absence of both $a = 0$ and $\lambda \to 0$ and AdS Schwarzschild BH when $Q = 0$, $a = 0$ and $\lambda \to 0$.

Exploiting the relation $T_+ = \frac{f'(r)}{4\pi}$, the Hawking temperature of the BH is calculated by

$$T_+ = \frac{1}{4\pi r_+}\left(1 - a + \frac{3r_+^2}{l^2} - \frac{Q^2}{r_+^2} + \frac{\lambda}{r_+}\right). \tag{22}$$

This temperature (22) identifies with the AdS charged Letelier BH mass in the limit of scale parameter $\lambda = 0$ as

$$T_+ = \frac{1}{4\pi r_+}\left(1 - a + \frac{3r_+^2}{l^2} - \frac{Q^2}{r_+^2}\right). \tag{23}$$

However, this reduces to AdS Letelier BH with PFDM when the charge is switched off as

$$T_+ = \frac{1}{4\pi r_+}\left(1 - a + \frac{3r_+^2}{l^2} + \frac{\lambda}{r_+}\right). \tag{24}$$

The BH temperature reduces to AdS Letelier BH mass in the absence of $Q = 0$ and $\lambda \to 0$, AdS Reisner Nordström BH in the absence of $a = 0$ and $\lambda = 0$ and AdS Schwarzschild BH when $Q = 0$, $a = 0$ and $\lambda \to 0$.

The plot of temperature for various values of the CoS parameter and scale parameter is depicted in Fig. 2, which shows that first temperature grows the maximum value (T_{Max}) and then reaches the minimum value and again increase (see the Fig. 2). In Fig. 2, we noticed that the temperature of the BH decreases when the CoS parameter is increasing, and the temperature of the BH increases with increases in the scale parameter. So, we can say that the behavior of the CoS and scale parameters on temperature are opposite.

The entropy of the resulting BH solution (19) is calculated using the first law of thermodynamics

$$dM_+ = T_+ dS_+ + \Phi dQ + \lambda d\Lambda_1 + PdV, \tag{25}$$

where Λ_1 is conjugate to λ.

At the constant charge (Q), the entropy of the given BH is calculated by

$$S_+ = \int \frac{1}{T_+}\frac{dM_+}{dr_+}dr_+ = \pi r_+^2 = \frac{A}{4}. \tag{26}$$

This entropy follows the area law and the corresponding Smarr relation is

$$M = 2TS - 2PV + \Phi Q + \lambda\Lambda_1, \tag{27}$$

with explicit expressions:

$$\Phi = \frac{dM_+}{dQ} = \frac{Q}{r_+}, \qquad V = \frac{4}{4}\pi r_+^3, \tag{28}$$

$$\Lambda_1 = -\frac{1}{2} + \frac{1}{2}\log\left[\frac{r_+}{\lambda}\right]. \tag{29}$$

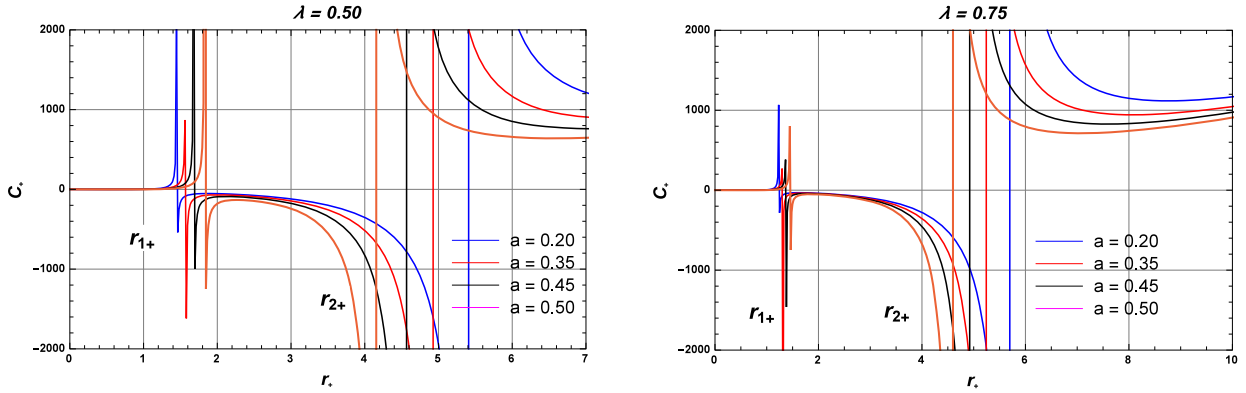

Fig. 3. The plot of C_+ versus the horizon radius r_+ for various values of the CoS parameter. In the left panel, we consider $a = 0.20$ (Blue line), $a = 0.345$ (Red line), $a = 0.45$ (Black line), and $a = 0.50$ (Pink line) with a fixed scale parameter $\lambda = 0.5$. In the right panel, we consider the same values of a with a fixed scale parameter $\lambda = 0.75$. Both cases are plotted for fixed values of $M = Q = 1$ and $l = 10$.

The stability of the BH is determined by the nature of heat capacity (C_+) and Gibbs free energy (G_+). Positive C_+ and negative G_+ confirm that BH solution is stable; however, negative C_+ and positive G_+ assures that the BH solution is unstable. The following relation can calculate the heat capacity:

$$C_+ = \frac{dM_+}{dT_+} = \frac{dM_+}{dr_+}\frac{dr_+}{dT_+}. \tag{30}$$

Substituting the value of mass and temperature from Eqs. (21) and (22) into Eq. (30), the heat capacity of the given BH solution is obtained as

$$C_+ = \frac{2\pi r_+^2(3r_+^2 - l^2(Q^2 - r_+(r_+ - ar_+ + \lambda)))}{3r_+^4 + l^2(3Q^2 + r_+(ar_+ - r - 2\lambda))}. \tag{31}$$

The expression (31) reduces to the heat capacity of Letelier BH with PFDM in the absence of charge as

$$C_+ = \frac{2\pi r_+^2(3r_+^2 + l^2(r_+(r_+ - ar_+ + \lambda)))}{3r_+^4 + l^2(r_+(ar_+ - r - 2\lambda))}. \tag{32}$$

The heat capacity reduces to AdS charged Letelier BH for $\lambda = 0$ as

$$C_+ = \frac{2\pi r_+^2(3r_+^2 - l^2(Q^2 - r_+(r_+ - ar_+)))}{3r_+^4 + l^2(3Q^2 + r_+(ar_+ - r))}. \tag{33}$$

The heat capacity 3 interpolates with the AdS charged BH in the limit $a = 0, \lambda \to 0$ and AdS Schwarzschild BH in the limit $Q = 0, a = 0$ and $\lambda \to 0$. In the plot Fig. 3, we can see that the heat capacity diverges at two points $r_1 = 0.47$ and $r_{2+} = 4.48$ for $\lambda = 0.50$ and $r_+ = 1.29$ and $r_{2+} = 5.31$ for $\lambda = 0.75$, respectively. Also, we notice that, in the intermediate region ($r_{2+} < r > r_{1+}$), the heat capacity decreases with increases in the CoS parameter. However, heat capacity increased with the scale parameter in this intermediate region.

One can use the standard relation, $G_+ = M_+ - T_+S_+$, to derive the Gibbs free energy. Plugging the values of mass, temperature, and entropy from Eq. (21), (22) and (26), respectively, into the relation, the Gibbs free energy of this BH solution is estimated by

$$G_+ = \frac{1}{4}\left(r_+ - ar_+ - \lambda + \frac{3Q^2}{r_+} - \frac{r_+^3}{l^2} + 2\log\left[\frac{r_+}{\lambda}\right]\right). \tag{34}$$

This expression reduces to the Gibbs free energy of charged Letailier BH with PFDM in the absence of charge

$$G_+ = \frac{1}{4}\left(r_+ - ar_+ - \lambda - \frac{r_+^3}{l^2} + 2\log\left[\frac{r_+}{\lambda}\right]\right). \tag{35}$$

To study the nature of Gibbs free energy and do a comparative analysis, we plot Fig. 4 for different values of CoS parameter (a) with fixed values of scale parameter ($\lambda = 0.50$ and $\lambda = 0.75$). From the figure, we see that the Gibbs free energy has local minima and local maxima at horizon radii $r_{1+} = 0.18$ and $r_+ = 6.1$ for $\lambda = 0.50$ and horizon radii $r_{1+} = 0.14$ and $r_+ = 5.1$ for $\lambda = 0.50$, respectively, where the heat capacity diverges (see Fig. 3). The temperature attains the extreme values (see Fig. 2). We also noticed that the BH gets early stability on the significant scale and CoS parameter values.

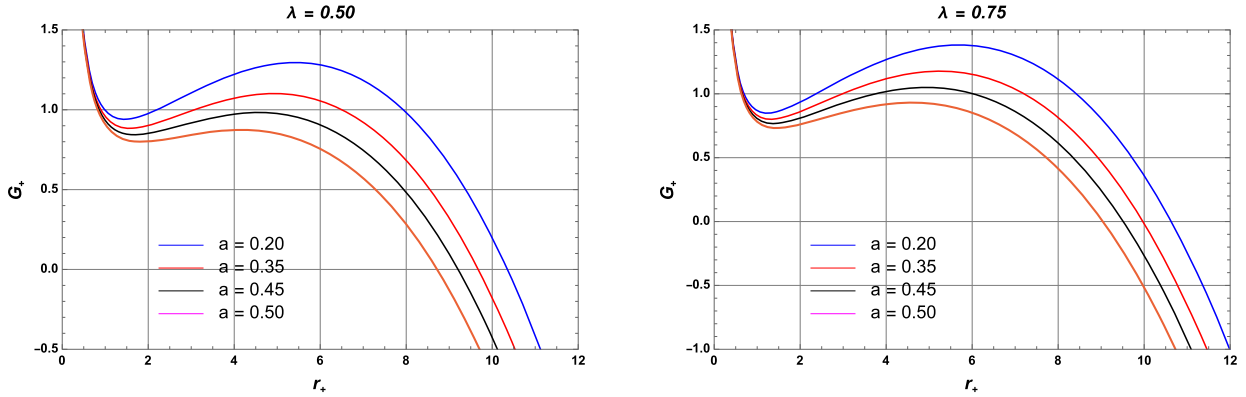

Fig. 4. The plot of Gibbs free energy G_+ versus the horizon radius r_+ for various values of the CoS parameter. In the left panel, we consider $a = 0.20$ (Blue line), $a = 0.345$ (Red line), $a = 0.45$ (Black line), and $a = 0.50$ (Pink line) with a fixed scale parameter $\lambda = 0.5$. In the right panel, we consider the same values of a with a fixed scale parameter $\lambda = 0.75$. Both cases are plotted for fixed values of $M = Q = 1$ and $l = 10$.

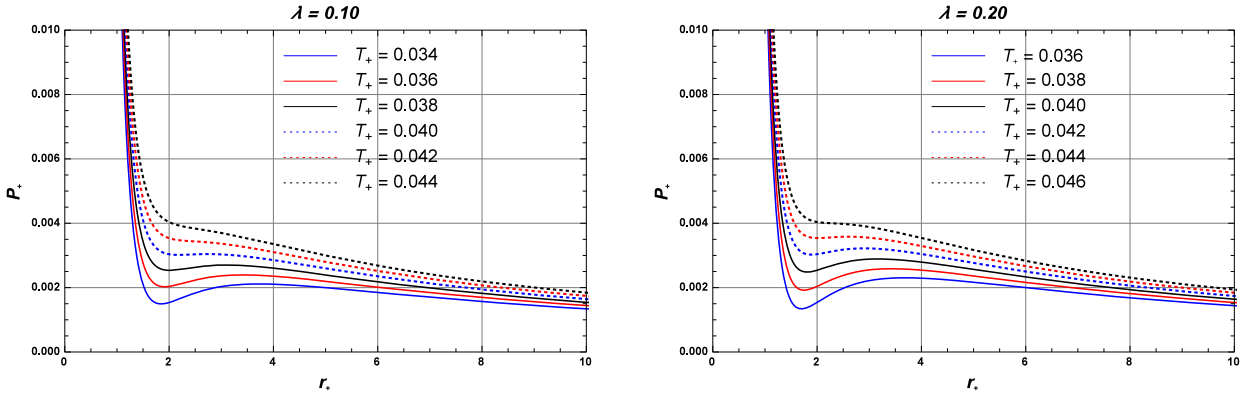

Fig. 5. The plot of pressure P_+ versus the horizon radius r_+ for different values of temperature. In the left panel, we consider $T_+ = 0.34$ (Blue line), $T_+ = 0.36$ (Red line), $T_+ = 0.38$ (Black line), $T_+ = 0.40$ (Dotted blue line), $T_+ = 0.42$ (Dotted red line), and $T_+ = 0.044$ (Dotted black line) with a fixed PFDM field parameter $\lambda = 0.50$. In the right panel, we consider $T_+ = 0.36$ (Blue line), $T_+ = 0.38$ (Red line), $T_+ = 0.40$ (Black line), $T_+ = 0.42$ (Dotted blue line), $T_+ = 0.44$ (Dotted red line), and $T_+ = 0.046$ (Dotted black line) with a fixed PFDM field parameter $\lambda = 0.75$. Both cases are plotted for a fixed CoS parameter $a = 0.1$ and charge $Q = 1$.

4. $P - v$ criticality, critical points and phase transition

In extended-phase space thermodynamics, the cosmological constant is treated as the thermodynamic pressure, and the mass of the BH is enthalpy. (See Fig. 5.) Using the expression of temperature (22), the EoS for pressure is given by

$$P = \frac{T_+}{2r_+} + \frac{Q^2}{8\pi r_+^2} + \frac{a}{8\pi r_+^2} - \frac{1}{8\pi r_+^2} - \frac{\lambda}{8\pi r_+^3}, \tag{36}$$

and the corresponding conjugate volume is expressed as

$$V_+ = \frac{4\pi}{3} r_+^3. \tag{37}$$

Now, we use the following inflection point conditions:

$$\frac{\partial P}{\partial r_+} = \frac{\partial^2 P_+}{\partial r_+^2} = 0, \tag{38}$$

and obtain the critical points as

$$r_c = \frac{3\lambda - \sqrt{24(1-a)Q^2 + 9\lambda^2}}{2(a-1)}, \tag{39}$$

$$T_c = \frac{2r_c^2 - 4Q^2 - 2ar_c^2 + 3r_c\lambda}{4\pi r_c^2}, \tag{40}$$

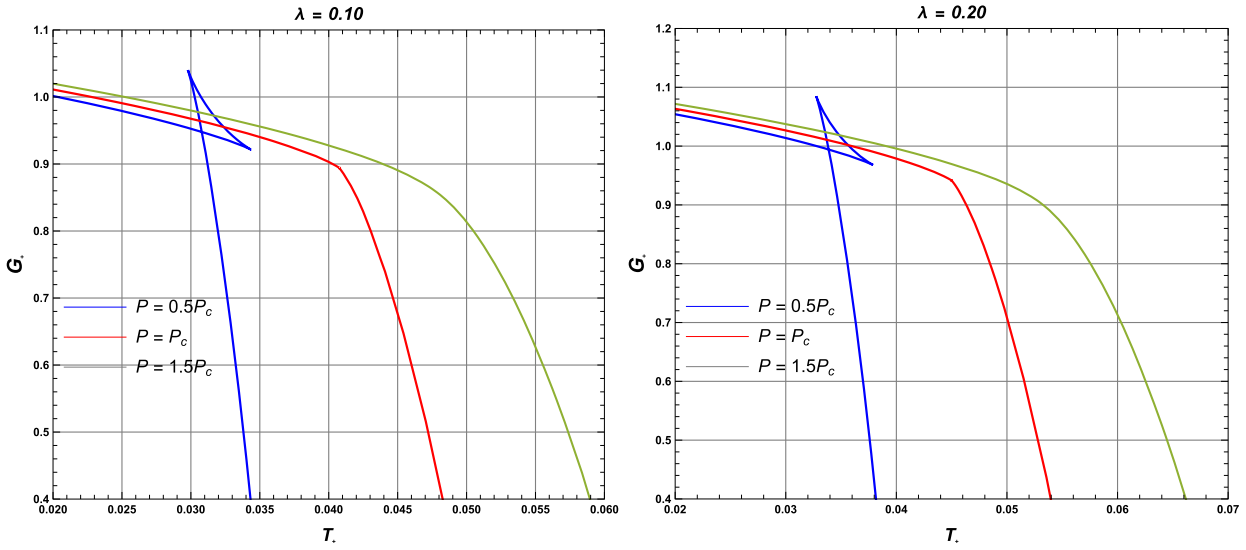

Fig. 6. The plot of Gibbs free energy versus temperature for various pressure values. In the left panel, we consider $P < P_c$ (Blue line), $P = P_c$ (Red line), and $P > P_c$ (Cyan line) for $\lambda = 0.10$. In the right panel, we consider the same pressure values for $\lambda = 0.20$. Both cases are plotted for $a = 0.1$ and $Q = 1$.

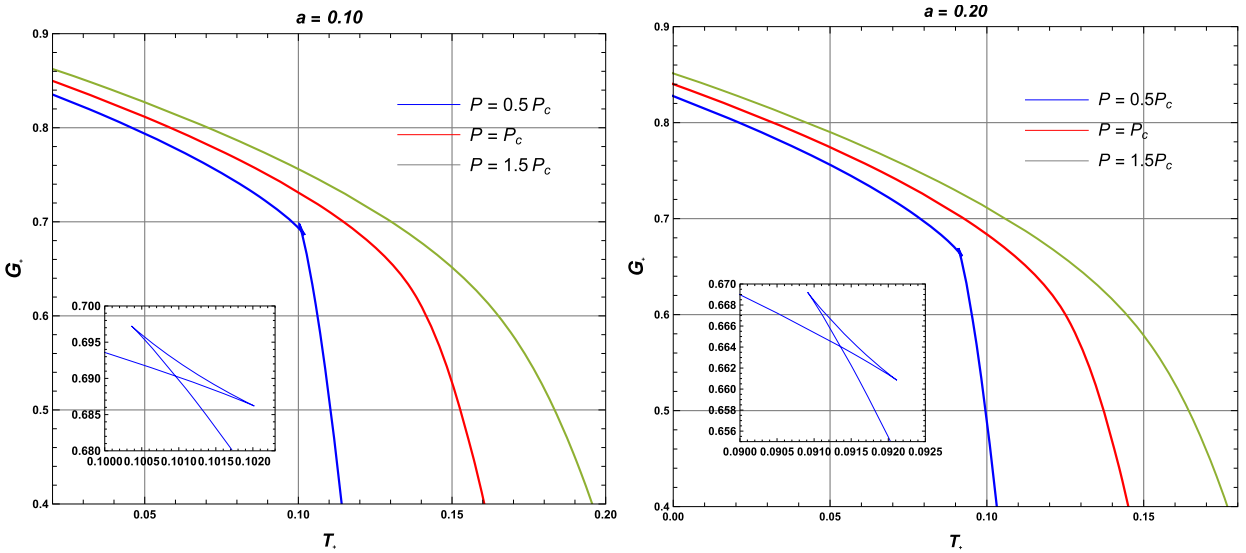

Fig. 7. The plot of Gibbs free energy versus temperature for various pressure values. In the left panel, we consider $P < P_c$ (Blue line), $P = P_c$ (Red line), and $P > P_c$ (Cyan line) for $\lambda = 0.50$. In the right panel, we consider the same pressure values for $\lambda = 0.75$. Both cases are plotted for $a = 0.1$ and $Q = 1$.

$$P_c = \frac{Q^2 - r_c^2 + a r_c^2 + 4\pi r_c^3 T_c - r_c \lambda}{8\pi r_c^4}. \tag{41}$$

These critical points reduce to the essential points of Reissner-Nordström BH without the CoS parameter and scale parameter.

Now, to study the phase transition, we plot $G_+ - T_+$ diagrams. In $G_+ - T_+$ plots, the appearance of characteristic swallow tail shape shows the phase transition points. In the Fig. 6, we see that swallow tail shape occurs at $P < P_c$ for the first-order phase transition and $\lambda = 0.10$ and $\lambda = 0.20$ with a fixed value of $a = 0.10$, the second-order phase transition occurs at $P = P_c = 0.00319$ and $P = P_c = 0.00339$, respectively. In the Fig. 7, a first-order phase transition occurs at $P < P_c = 0.0276$ for $a = 0.10$ and $P = P_c = 0.0248$ for $a = 0.20$ with a fixed value of $\lambda = 1$.

From the Fig. 6 and Fig. 7 for specific scale and CoS parameters and a certain range of pressure, we observe that there are three kinds of BHs, namely, small ($P < P_c$), intermediate ($P = P_c$) and large BH ($P > P_c$). Here, the small and large BHs are more stable than the intermediate BH, which is unstable due to negative heat capacity (see Fig. 3). We can see a transition temperature $T_\star$ at which BH transits from one phase to another due to the same free energy. The values of transit temperature are $T_\star = 0.0307$ and $T_\star = 0.0339$ for $\lambda = 0.10$ and $\lambda = 0.20$ with fixed value of CoS parameter ($a = 0.1$), respectively and the $T_\star = 0.109$ and $T_\star = 0.093$ for $a = 0.10$ and $a = 0.20$ with fixed value of scale parameter ($\lambda = 1.0$), respectively. We can say that the transition temperature increases

with λ and decreases with a. In Fig. 6. isotherms represent the first-order phase transition at $T_+ = T_\star$ and the second-order phase transition at $T_+ = T_c$, 4. At $T_+ < T_\star$, the small BH occurs, and at $T_+ > T_\star$, large BH occurs due to small free energy.

5. Conclusion

An exact BH solution was found within the framework incorporating the CoS parameter, surrounded by the PFDM field. This BH solution had interpolated between well-known BH models. Specifically, in the absence of the CoS and scale parameters, the solution had reduced to the Reissner-Nordström BH, a charged solution in an asymptotically flat spacetime. Additionally, when the electric charge, the CoS parameter, and the scale parameter were set to zero, the solution was simplified to the Schwarzschild BH, an uncharged, spherically symmetric solution.

The size of the BH had been shown to depend on both the CoS parameter and the PFDM field. As the CoS parameter had increased, the size of the BH correspondingly increased, whereas the PFDM field acted to decrease the BH size. This relation indicates that the two parameters exert opposite influences on spacetime's geometry and BH's horizon structure.

Moreover, a comprehensive study of the BH thermodynamic properties was conducted. This study included an analysis of quantities such as mass, temperature, heat capacity, and free energy. It had been observed that the heat capacity diverged at the extremum points of temperature and Gibbs free energy, indicating the presence of critical phenomena and phase transitions within the system.

In addition to the thermodynamic study, the BH's critical points and phase structure were analyzed using EoS and Gibbs free energy. The analysis revealed that the CoS parameter and the PFDM field had opposite effects on the critical points. Specifically, while the CoS parameter had decreased the critical temperature and pressure, the PFDM field had increased these critical values. This behavior highlights the competing effects of the CoS parameter and the PFDM field on the BHs thermodynamics.

Furthermore, three phases of BHs had been identified, depending on the pressure relative to the critical pressure (P_c). For pressures below the critical pressure ($P < P_c$), small stable BHs had been observed. For pressures above the critical pressure ($P > P_c$), large stable BHs had been present, while in the crucial pressure ($P = P_c$), intermediate unstable BHs had emerged. This classification of phases illustrated the complexity of the BH phase structure in terms of varying pressure conditions.

The emergence of a shallow tail structure in the $G_+ - T_+$ (Gibbs free energy versus temperature) diagram provided further evidence of a first-order phase transition occurring at the transition temperature. Additionally, it had been observed that the transition temperature decreased with an increase in the scale parameter, indicating that it had played a significant role in regulating the dynamics of the phase transition. These findings contributed to a deeper understanding of the phase behavior and critical phenomena in BH systems influenced by both the CoS parameter and the PFDM field.

Declaration of competing interest

The authors declare that they have no known competing financial interests or personal relationships that could have appeared to influence the work reported in this paper.

Acknowledgements

This research was funded by the Science Committee of the Ministry of Science and Higher Education of the Republic of Kazakhstan (Grant No. AP23487178). D.V.S. would like to thank DST-SERB under project no. EEQ/2022/000824 and IUCAA, Pune, for hospitality while this work was carried out.

Data availability

No data was used for the research described in the article.

References

[1] J.D. Bekenstein, Phys. Rev. D 7 (1973) 2333.
[2] J.M. Bardeen, B. Carter, S.W. Hawking, Commun. Math. Phys. 31 (1973) 61.
[3] S.W. Hawking, Commun. Math. Phys. 43 (1975) 99; 46 (1976) 206(E).
[4] S.W. Hawking, D.N. Page, Commun. Math. Phys. 87 (1983) 577.
[5] J.M. Maldacena, Adv. Theor. Math. Phys. 2 (1998) 231.
[6] E. Witten, Adv. Theor. Math. Phys. 2 (1998) 253.
[7] A. Chamblin, R. Emparan, C.V. Johnson, R.C. Myers, Phys. Rev. D 60 (1999) 104026.
[8] A. Chamblin, R. Emparan, C.V. Johnson, R.C. Myers, Phys. Rev. D 60 (1999) 06401.
[9] M.M. Caldarelli, G. Cognola, D. Klemm, Class. Quantum Gravity 17 (2000) 399.
[10] D. Kastor, S. Ray, J. Traschen, Class. Quantum Gravity 26 (2009) 195011.
[11] B.P. Dolan, Class. Quantum Gravity 28 (2011) 125020.
[12] D. Kubiznak, R.B. Mann, J. High Energy Phys. 07 (2012) 033.
[13] D.V. Singh, V.K. Bhardwaj, S. Upadhyay, Eur. Phys. J. Plus 137 (2022) 969.
[14] B.K. Singh, R.P. Singh, D.V. Singh, Eur. Phys. J. Plus 136 (2021) 575.
[15] P. Paul, S. Upadhyay, Y. Myrzakulov, D.V. Singh, K. Myrzakulov, Nucl. Phys. B 993 (2023) 116259.
[16] S. Upadhyay, D.V. Singh, Eur. Phys. J. Plus 137 (2022) 383.
[17] Y. Myrzakulov, K. Myrzakulov, S. Upadhyay, D.V. Singh, Int. J. Geom. Methods Mod. Phys. 20 (2023) 2350121.

[18] D.V. Singh, S. Siwach, Phys. Lett. B 808 (2020) 135658.
[19] B. Singh, B.K. Singh, D.V. Singh, Int. J. Geom. Methods Mod. Phys. 20 (2023) 23501.
[20] H.K. Sudhanshu, D.V. Singh, S. Upadhyay, Y. Myrzakulov, K. Myrzakulov, Phys. Dark Universe 46 (2024) 101648.
[21] A. Kumar, D.V. Singh, S. Upadhyay, Int. J. Mod. Phys. A 39 (2024) 2450136.
[22] S.H. Hendi, S. Hajkhalili, M. Jamil, M. Momennia, Eur. Phys. J. C 81 (2021) 1112.
[23] N. Altamirano, D. Kubizňák, R.B. Mann, Z. Sherkatghanad, Galaxies 2 (2014) 89–159.
[24] S. Upadhyay, N. Ul-Islam, P.A. Ganai, JHAP 2 (2022) 25.
[25] D.V. Singh, S. Upadhyay, S. Ali, Int. J. Mod. Phys. A 37 (2022) 2250049.
[26] G.A. Marks, F. Simovic, R.B. Mann, Phys. Rev. D 104 (2021) 104056.
[27] D.V. Singh, B.K. Singh, S. Upadhyay, Ann. Phys. 434 (2021) 168642.
[28] B.K. Singh, R.P. Singh, D.V. Singh, Eur. Phys. J. Plus 135 (2020) 862.
[29] S.H. Hendi, R.B. Mann, S. Panahiyan, B. Eslam Panah, Phys. Rev. D 95 (2017) 021501.
[30] J. Wu, R.B. Mann, Phys. Rev. D 107 (2023) 084035.
[31] J. Wu, R.B. Mann, Class. Quantum Gravity 40 (2023) 145009.
[32] J. Wu, R.B. Mann, Class. Quantum Gravity 40 (6) (2023) 06LT01.
[33] M. Tavakoli, J. Wu, R.B. Mann, J. High Energy Phys. 12 (2022) 117.
[34] A.M. Frassino, R.B. Mann, F. Simovic, arXiv:1611.03525 [hep-th].
[35] D. Astefanesei, P. Cabrera, R.B. Mann, R. Rojas, Phys. Rev. D 105 (4) (2022) 046021.
[36] R.A. Hennigar, R.B. Mann, E. Tjoa, Phys. Rev. Lett. 118 (2017) 021301.
[37] R.A. Hennigar, R.B. Mann, Entropy 17 (2015) 8056–8072.
[38] S.G. Ghosh, A. Kumar, D.V. Singh, Phys. Dark Universe 30 (2020) 100660.
[39] S.G. Ghosh, D.V. Singh, R. Kumar, S.D. Maharaj, Ann. Phys. 424 (2021) 168347.
[40] D.V. Singh, S.G. Ghosh, S.D. Maharaj, Phys. Dark Universe 30 (2020) 100730.
[41] D.V. Singh, A. Shukla, S. Upadhyay, Ann. Phys. 447 (2022) 169157.
[42] P.S. Letelier, Phys. Rev. D 20 (1979) 1294.
[43] P.S. Letelier, Nuovo Cimento B 63 (1981) 519–528.
[44] P.S. Letelier, Phys. Rev. D 28 (1983) 2414.
[45] S.G. Ghosh, U. Papnoi, S.D. Maharaj, Phys. Rev. D 90 (4) (2014) 044068.